CrystEngComm

ROYAL SOCIETY OF CHEMISTRY

PAPER

View Article Online
View Journal | View Issue

Cite this: *CrystEngComm*, 2022, **24**, 3537

Enhanced luminescence of single-benzene fluorescent molecules through halogen bond cocrystals†

Fei Yu,[ab] Xiunan Zhang,[ab] Hongtu Zhao,[ab] Zhicheng Jiang,[ab] Ting Wang,*[ab] Na Wang,[ab] Xin Huang,[ab] Lina Zhou[ab] and Hongxun Hao*[abc]

Received 17th February 2022,
Accepted 1st April 2022

DOI: 10.1039/d2ce00229a

rsc.li/crystengcomm

Organic single benzene fluorescent molecules often suffer from an aggregation-induced quenching effect under solid-state conditions, especially for red-emissive molecules, due to their flat rigid molecular framework and strong π–π interactions. Cocrystal engineering is expected to be a useful tool that can change the packing arrangement and intermolecular interactions inside a crystal through different molecular self-assembly arrangements, which might endow materials with more excellent properties. In this study, two cocrystals of a single benzene X-type luminescent molecule dimethyl 2,5-bis((3-chloropropyl)amino)-terephthalate (DMCAT), namely DMCAT-1 and DMCAT-2, were prepared. Both cocrystals exhibit red shifts relative to DMCAT form II (10 nm and 16 nm) and significantly increased quantum yields (approximately 3 and 5 times). By combining solid-state characterization and theoretical analysis, the mechanism of photophysical property changes and the driving force of molecular self-assembly were explored. It was found that the introduction of co-former molecules weakens the π–π interaction between the DMCAT molecules, thus attenuating the aggregation-induced quenching effect, resulting in enhanced emission.

1. Introduction

In recent decades, modern photochemistry has developed rapidly with increasing attention to energy, environment, and health issues.[1] In particular, as one of the most cutting-edge research topics, luminescent organic materials have attracted strong interest due to their potential applications in the fields of organic light-emitting diodes (OLEDS), biological imaging, organic solid-state lasers, chemical sensors, *etc.*[2–7] Meanwhile, high-emission efficiency in the solid state is an extremely important prerequisite for the applications of such desired devices with superior performance.[8] Common organic fluorescent scaffolds are mainly based on planar rigid extended π-conjugate systems or a push–pull system with a strong donor–π–acceptor framework.[9–11] Therefore, complex substituent modifications and cumbersome synthesis steps are usually required in order to achieve efficient emission. With the development of supramolecular chemistry and crystal engineering, multi-component molecular materials such as cocrystals have been extensively studied.[12–17] Organic cocrystals are usually assembled by two or more different molecules in a clear stoichiometric ratio through non-covalent interactions, such as hydrogen bonds, halogen bonds, and π–π stacking interactions.[12,18,19] Cocrystal engineering can avoid complex synthetic procedures, and it is easy to manipulate non-covalent interactions between molecules to achieve adjustable functional properties, providing a good platform for revealing the structure–property relationship at the molecular level.[12,13] Cocrystal engineering has been developed as an effective strategy for adjusting optical properties. For example, Xu *et al.* reported a cocrystal composed of luminescent molecule BP4VA and halogen co-former FIB, which can achieve a crystal phase transition from yellow to green under the conditions of THF vapor, thermal stimulation and mechanical grinding.[12] Hu *et al.* successfully prepared a charge-transfer (CT) cocrystal of *trans*-1,2-diphenylethylene (TSB) and 1,2,4,5-tetracyanobenzene (TCNB) and observed thermally activated delayed fluorescence (TADF) in the cocrystal for the first time.[20] Li *et al.* discovered a self-assembled organic cocrystal of *N*,*N*,*N*′,*N*′-tetramethyl-*p*-phenylenediamine (TMPD) and pyromellitic dianhydride

[a] *National Engineering Research Center of Industrial Crystallization Technology, School of Chemical Engineering and Technology, Tianjin University, Tianjin 300072, China. E-mail: hongxunhao@tju.edu.cn*
[b] *Collaborative Innovation Center of Chemical Science and Engineering (Tianjin), Tianjin 300072, China*
[c] *School of Chemical Engineering and Technology, Hainan University, Haikou 570208, China*

† Electronic supplementary information (ESI) available: Details of the crystallographic parameters, CIF files and two cocrystals DMCAT-I and DMCAT-II. CCDC 2162957 and 2162959. For ESI and crystallographic data in CIF or other electronic format see DOI: **https://doi.org/10.1039/d2ce00229a**

(PMDA), with high near-infrared photothermal conversion efficiency.[21]

As small π-conjugated systems, single benzene luminescent molecules have attracted considerable research attention in the past few years due to their excellent properties and easy preparation. For instance, Zhang *et al.* found two polymorphs of 2,5-bis((thiophen-2-ylmethyl)amino)-dimethyl terephthalate crystals exhibiting a flexible optical waveguide.[22] Liu proposed a unique asymmetric monophenyl chromophore with effective emission, large Stokes shift and significant ratio-dependent pH-dependent fluorescence.[23] X-shaped tetrasubstituted benzene is a special type of single benzene luminescent molecule, in which two electron donating groups (EDGs) and two electron withdrawing groups (EWGs) are connected to the benzene ring and arranged in an X shape.[24] However, such a small π-system usually means lower radiative transition rates, resulting in low emission efficiency, especially for red luminescent molecules.[24–26] Therefore, how to effectively avoid π–π stacking and dipole–dipole interactions to achieve strong fluorescence emission is still a big challenge. Considering the advantages of cocrystal engineering,[4] it could be speculated that it is possible to endow fluorescent molecular materials with excellent performance by incorporating co-former molecules to change the intermolecular interactions and stacking modes in the solid state.

In this work, dimethyl 2,5-bis((3-chloropropyl)amino)-terephthalate (DMCAT) was selected as a typical X-type single benzene luminescent model compound.[26] By choosing different halogen bond donors (1,4-diiodotetrafluorobenzene named co-former 1 and 1,4-dibromotetrafluorobenzene named co-former 2), two cocrystal systems with enhanced emission efficiency were synthesized. Here, the optical properties (such as emission wavelength, lifetime, and quantum yield) of the two cocrystals were characterized and evaluated. It was found that the different optical properties are derived from the changes in molecular packing and interactions in the two cocrystals. By combining SXRD, IR, Hirshfeld surfaces, electrostatic potential analysis and DFT calculation, the driving force for cocrystal formation and the relationship between photophysical behaviors and structures are discussed, which would provide guidance for the performance optimization of optical materials.

2. Experimental methods

2.1. Materials

Dimethyl 2,5-dioxocyclohexane-1,4-dicarboxylate (98%), 3-chloropropylamine hydrochloride (98%), ethanol (99%), and 4-(dimethylamino)pyridine (98%) were purchased from 3A Chemicals. 1,4-Dibromotetrafluorobenzene (1,4-DBTFB) and 1,4-diiodotetrafluorobenzene (1,4-DITFB) were purchased from Shanghai Bide Pharmaceutical Technology Co., Ltd. All of the materials were used without further purification.

2.2. Synthesis steps

Organic fluorescent compound dimethyl 2,5-bis((3-chloropropyl)amino)-terephthalate (DMCAT) was synthesized according to the method in the literature.[26] The DMCAT-1 cocrystal was obtained by evaporating an acetone solution (2 mL) of a DMCAT and co-former 1 mixture (at a molar ratio of 1 : 5). The preparation of DMCAT-2 is divided into two steps. First, a mixed solution (2 mL) of DMCAT and co-former 2 was prepared in a beaker at a molar ratio of 1 : 4, and then 10 mL of *n*-hexane was added dropwise along the inner wall of the beaker and the obtained solution was sealed with plastic wrap. Finally, the DMCAT-2 co-crystal was obtained by diffusion crystallization.

2.3. Characterization

PXRD measurements (R-AXIS RAPID, Rigaku, Japan) were performed with Cu-Kα radiation (1.5405 Å, 5–50°, 8° min^{-1}). SXRD (XtaLAB FRX, Rigaku, Japan) data were collected to analyze the crystal structures. The Fourier transform infrared spectrometry (FTIR) data for all the samples were measured using a Bruker Alpha FTIR-ATR instrument from 4000 to 400 cm^{-1} with a resolution of 4 cm^{-1}. Each spectrum was scanned 32 times. The thermal properties were characterized *via* differential scanning calorimetry (DSC, temperature range, 25–200 °C, 10 K min^{-1}, Mettler Toledo, Switzerland). The UV-vis absorption spectra were collected using a UV-3010 spectrophotometer (HITACHI, Japan). The fluorescence spectra, fluorescence lifetimes and quantum yields of the cocrystals were measured through an Edinburgh instrument (FLS1000, UK). The quantum yield was measured using the same excitation wavelength (450 nm) as that reported in the literature.[26]

2.4. Computational methods

All calculations involved were performed by Gaussian 09 packages. The B3LYP/6-311G(d,p) level was used to optimize the geometrical structure of the ground state. The maximum absorption wavelengths were obtained through time-dependent density functional theory (TD-DFT) at the B3LYP/TZVP level.

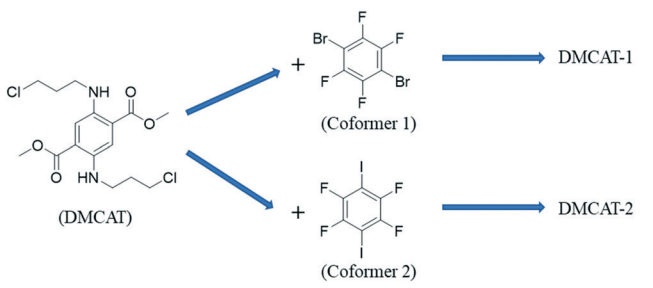

Fig. 1 Chemical structures of DMCAT, co-former 1, and co-former 2.

3. Results and discussion

3.1. Characterization of the two cocrystals of DMCAT

DMCAT is known to have two polymorphs (form I and form II)[26] and the chemical structures of DMCAT, co-former 1 and co-former 2 are shown in Fig. 1. Halogen bonding is one kind of noncovalent interaction similar to hydrogen bonding, which has been developed as an efficient way to rationally design organic cocrystals. The two co-formers contain rich halogen atoms that can act as halogen bond donors, so that they can be easily co-assembled into multicomponent crystals through electrostatic interactions with halogen bond acceptors (such as π-systems and O- and N-acceptors) provided by DMCAT molecules. Based on this, two new DMCAT cocrystals were successfully synthesized, namely DMCAT-1 and DMCAT-2. Fig. 2 shows the PXRD patterns of DMCAT, co-formers 1 and 2, and the two cocrystals. It can be found that the original peaks of raw materials vanish and new characteristic peaks appear, indicating the formation of new phases. For DMCAT-1, new diffraction peaks appear at 9.02°, 19.92°, and 21.83°, while the typical diffraction peaks of DMCAT and co-former 1 disappear. For DMCAT-2, new diffraction peaks appear at 9.1°, 11.62°, and 14.9°. Moreover, the PXRD patterns of the two cocrystals exhibit good agreement with the results obtained from the single crystal structure simulation, and they also show a certain similarity, suggesting that they might have a similar packing structure.[3] To further verify the formation of the cocrystals, differential scanning calorimetry (DSC) and thermogravimetric analysis (TGA) were performed. As shown in Fig. 3, the melting points of both DMCAT-1 and DMCAT-2 are different from the two polymorphs of DMCAT, due to new packing modes and intermolecular interactions after self-assembly, and no solvent removal or phase transformation can be observed. The TGA diagrams show that the decomposition temperatures of DMCAT-1 and DMCAT-2 are in between the decomposition temperatures of the two single components (around 88 °C and 121 °C, respectively), also suggesting the formation of a new phase.

3.2. Photophysical properties

The photophysical properties of the two cocrystals were tested. Compared with the two polymorphs of DMCAT, the absorption spectra of the two cocrystals exhibit red-shifted and broader absorption bands (Fig. 5a). To better understand the photophysical process, the transient DFT calculation based on background charge was performed at the B3LYP/TZVP level, and the calculation results are shown in Fig. 4. It can be seen that the HOMO–LUMO distribution of the DMCAT molecules in the two compounds are nearly the same, in which the HOMOs are mainly concentrated in the positions of the benzene ring and nitrogen atoms, and the LUMOs are mainly concentrated in the positions of the benzene ring and ester groups. In addition, no intermolecular charge transfer from DMCAT to the two co-formers was observed, indicating that the first excited state (S_1) is mainly caused by the intramolecular charge transfer transition from the HOMO to the LUMO. What's more, the simulated results show the absorption wavelength red-shift of DMCAT-1 (493 nm) relative to DMCAT-2 (484 nm), which is in good agreement with the experimental results.

Subsequently, the fluorescence emission spectra of the two cocrystals were obtained, as shown in Fig. 5(b). The emission wavelengths of the new cocrystals formed are 632 and 638 nm, respectively, which are red-shifted compared to those of the two crystalline forms of pure DMCAT. The corresponding CIE coordinates are (0.67, 0.33) and (0.69, 0.31), respectively, as shown in Fig. 5(e). Next, the excited state properties of the two cocrystals were studied by time-resolved spectroscopy (Fig. 5). Based on the tested lifetime and quantum yield, the radiative transition rate (k_r) and the nonradiative transition rate (k_{nr}) were calculated, as shown in Table 1. For the DMCAT-1 and DMCAT-2 cocrystals, the fluorescence quantum yields decrease slightly compared to that of the solution state of DMCAT, while the fluorescence quantum yields increase significantly compared to those of both polymorphs of DMCAT. Considering the longer emission wavelength, we mainly

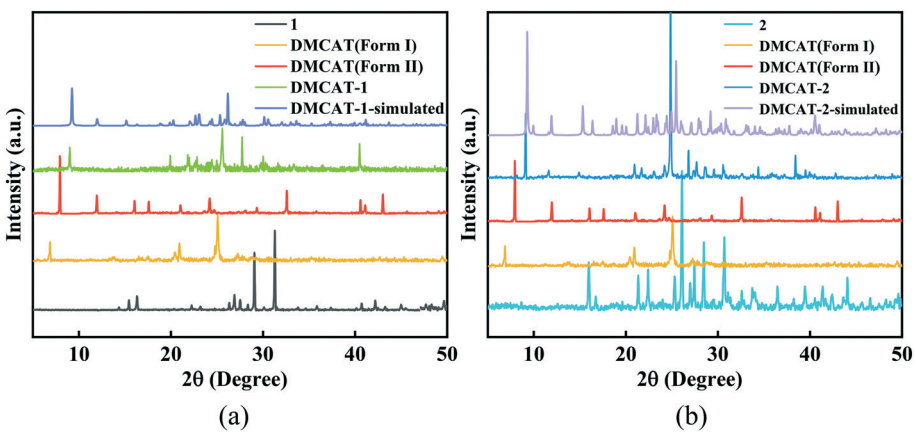

Fig. 2 PXRD patterns of (a) DMCAT-1 and (b) DMCAT-2, including the corresponding co-formers and two polymorphs of DMCAT.

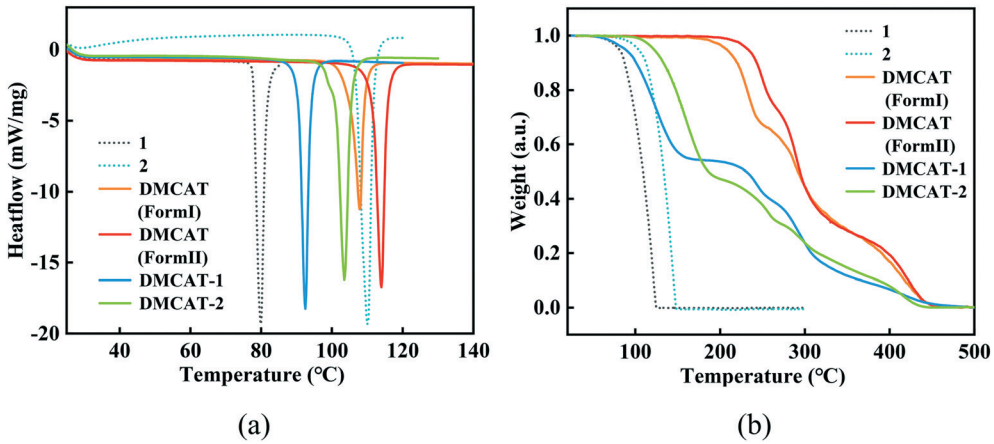

Fig. 3 (a) DSC and (b) TG patterns of the two cocrystals and their co-formers.

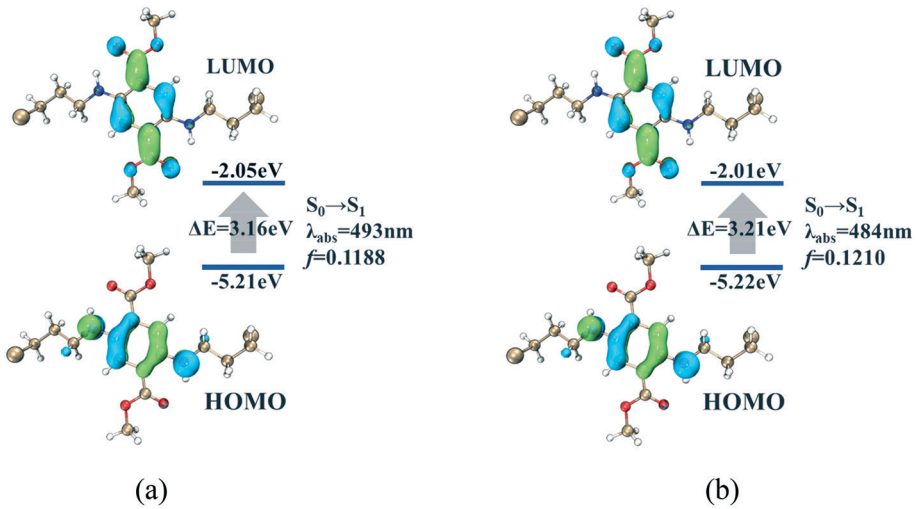

Fig. 4 Molecular orbital diagrams and simulated photophysical information for (a) DMCAT-1 and (b) DMCAT-2.

compared the properties of the two cocrystals with those of DMCAT form II. Compared with DMCAT form II, the calculated radiative transition rate of DMCAT-2 increases and the nonradiative transition rate decreases, resulting in increased quantum yields (about 5 times that of DMCAT form II). For DMCAT-1, the radiative transition rate is greater while the nonradiative transition rate is less compared with DMCAT form II, so the quantum yield increases to 3 times that of DMCAT form II. Despite similar packing structures of the two cocrystals, the luminous efficiency of DMCAT-2 is greater than that of DMCAT-1.

3.3. Cocrystal structure and interaction analysis

In general, different stacking modes can lead to different photophysical properties. To understand the underlying mechanism of these photophysical behaviors, single crystal X-ray diffraction analysis of the two cocrystals was performed. As illustrated in Fig. 6, DMCAT-1 and DMCAT-2 adopt similar mixed packing patterns and both belong to the $P\bar{1}$ space group with $Z = 1$ (Table 2). The DMCAT molecules in the two cocrystals exhibit almost the same molecular conformations and both have N–H···O intramolecular hydrogen bonds (2.037 Å in DMCAT-1 and 2.049 Å in DMCAT-2), ensuring the rigid planar structure in the DMCAT molecules. Both the co-former molecules form one-dimensional supramolecular chains along the *b* axis with DMCAT molecules through C–Br···O (or C–I···O) intermolecular halogen bonds and C–F···H intermolecular hydrogen bonds. The iodine atom in co-former 2 has stronger polarizability, so the halogen bond formed in DMCAT-2 is stronger than that of DMCAT-1 (the interaction distances in DMCAT-1 and DMCAT-2 are 3.118 Å and 3.083 Å, respectively). Adjacent chains are connected to molecular layers through C–F···H and C–Cl···H interactions, which are also the stronger interactions in the cocrystals. The adjacent molecular layers are connected along the *a* axis by π–π interactions and C–Br···H (or C–I···H) interactions, and finally form an ABAB mixed stacking pattern. The insertion of the co-former molecules can dilute the DMCAT molecules to a certain extent,[27] thereby inhibiting the π–π interactions

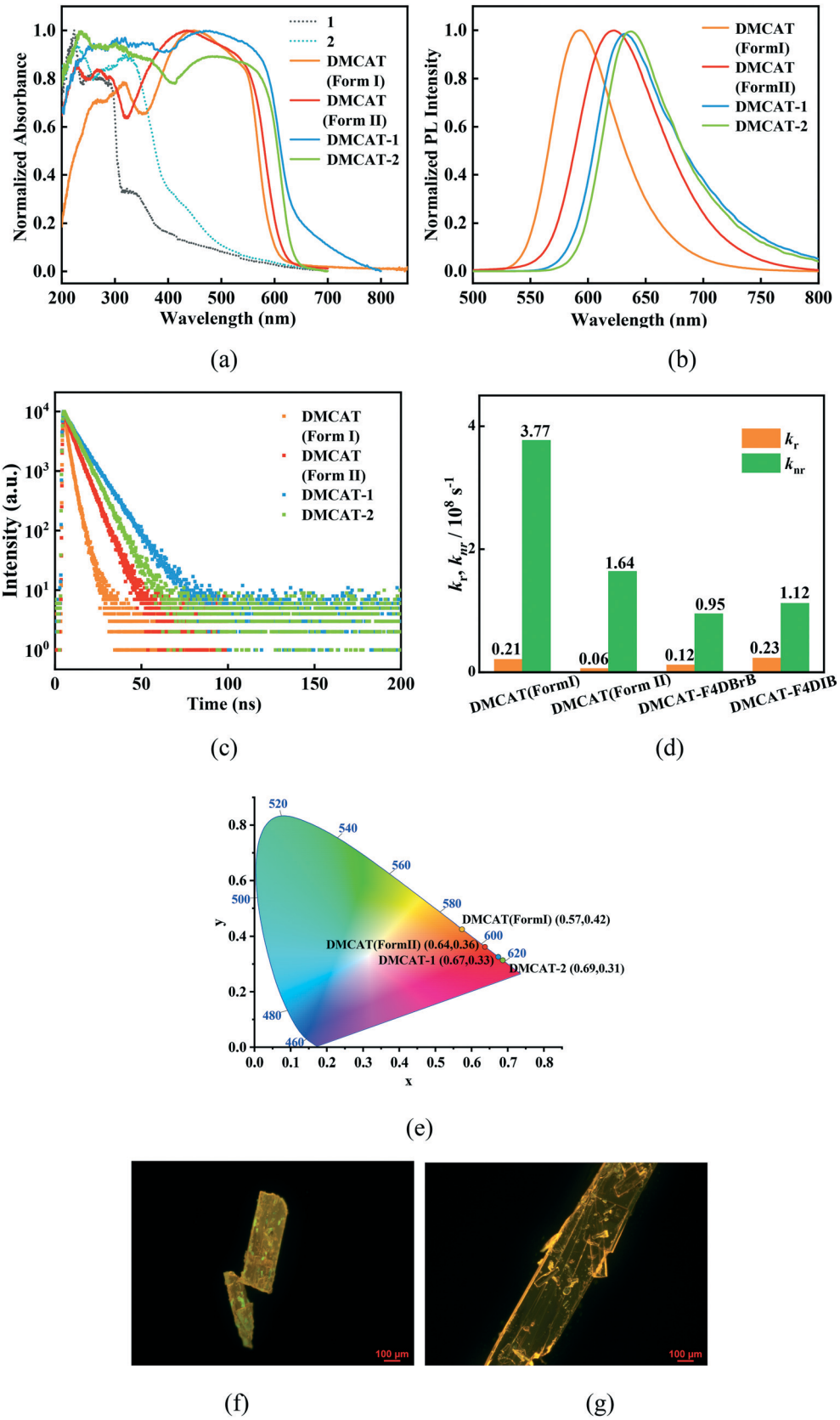

Fig. 5 (a) Absorption spectra, (b) normalized fluorescence spectra, (c) lifetimes, and (d) radiative transition rates (k_r) and nonradiative transition rates (k_{nr}). (e) The CIE coordinates according to the CIE 1931 chromaticity of the two polymorphs of DMCAT, DMCAT-1 and DMCAT-2; images of DMCAT-1 and DMCAT-2 under UV light (f) and (g) observed using a fluorescence microscope.

Table 1 The detailed photophysical data for DMCAT-1, DMCAT-2, and the two polymorphs of DMCAT

Name	λ_{em} (nm)	Φ_F (%)	τ (ns)	k_r (10^8 \s^{-1})	k_{nr} (10^8 s^{-1})
DMCAT (in acetone)	569	26.0	7.77	0.34	0.95
DMCAT (form I)	594	5.2	2.51	0.21	3.77
DMCAT (form II)	622	3.4	5.48	0.06	1.64
DMCAT-1	632	11.0	9.40	0.12	0.95
DMCAT-2	638	17.2	7.38	0.23	1.12

between the DMCAT luminescent molecules and attenuating the effect of aggregation-induced quenching effect. It is worth noting that each halogen atom on the benzene ring of the co-former molecule can form strong non-covalent interactions with the four adjacent DMCAT molecules, which is important for inhibiting the movement of DMCAT molecules in the crystal, thereby suppressing the nonradiative transition process. This is consistent with the previously calculated nonradiative transition rate constants of the cocrystals, which are greatly reduced compared with those of both of the DMCAT crystals, resulting in stronger emission. In addition, it should also be noted that the interaction distance between adjacent DMCAT molecules and co-former molecules in DMCAT-2 is longer (centroid–centroid distance: 3.706 Å for DMCAT-1 and 3.737 Å for DMCAT-2), indicating weaker π–π interactions between them. Therefore, the aggregation-induced quenching effect is weaker, resulting in stronger emission and higher quantum yield in DMCAT-2. At the same time, a red-shift in the emission wavelength of both cocrystals compared to the DMCAT crystals (red-shifted by 10 nm and 16 nm, respectively, compared to DMCAT (form II)) can be noticed. A possible reason for this phenomenon is the formation of stronger π–π stacking interactions in the cocrystals.

As described above, by employing similar co-former molecules, two cocrystals with a similar crystal structure were prepared. However, they are different from the results reported recently by Hu *et al.* in 2021.[27] The cocrystals in the reported paper showed two different packing modes (mixed stack and segregated stack patterns, respectively), where 1,4-dibromotetrafluorobenzene and 1,4-diiodotetrafluorobenzene are used as co-former molecules. Although their co-former molecules are the same with ours, the fluorescent molecules have many structural differences. The fluorescent molecule reported has a polyaromatic ring structure, which easily leads to the fact that the crystal contains not only interactions between fluorescent molecules and co-former molecules such as C–X···N, C–F···H and π···π interactions, but also strong interactions between fluorescent molecules, such as C–H···N, C–H···C, and π···π interactions. These multiple interactions can cooperate with each other and affect the arrangement of molecules within the crystal. Besides, for the DPYA-IFB

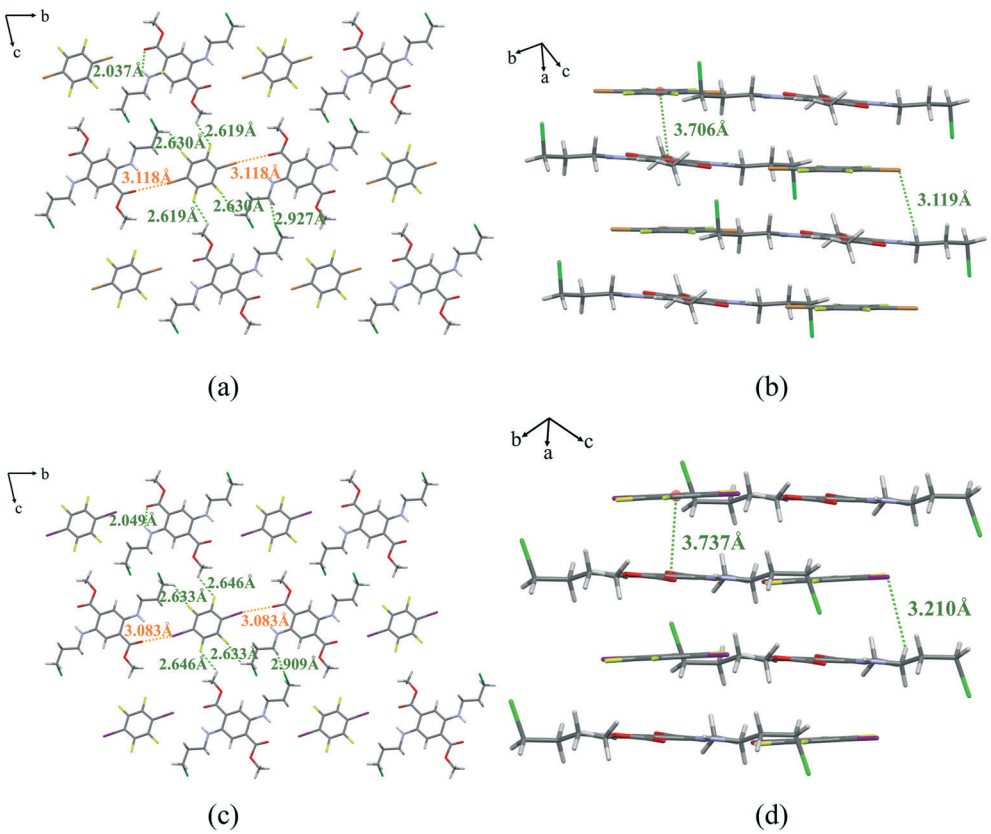

Fig. 6 Multiple intra/intermolecular contacts between adjacent molecules (hydrogen bonds are marked with green dashed lines; halogen bonds are marked with orange dashed lines) and π–π packing images of DMCAT-1 (a) and (b) and DMCAT-2 (c) and (d).

Table 2 Crystallographic data and refinement details for DMCAT-1 and DMCAT-2

Name	DMCAT-1	DMCAT-2
Empirical formula	$C_{22}H_{22}Br_2Cl_2F_4N_2O_4$	$C_{22}H_{22}Cl_2F_4I_2N_2O_4$
Formula weight	685.13	779.11
Temperature/K	113.15	113.15
Crystal system	Triclinic	Triclinic
Space group	$P\bar{1}$	$P\bar{1}$
a/Å	7.4110(3)	7.4734(2)
b/Å	9.0343(6)	9.3123(5)
c/Å	9.7976(6)	9.9081(4)
α/°	76.870(5)	73.840(4)
β/°	88.723(5)	86.669(3)
γ/°	84.956(4)	82.978(3)
Volume/Å^3	636.36(6)	657.13(5)
Z	1	1
ρ_{calc} g cm^{-3}	1.788	1.969
μ/mm^{-1}	3.457	2.657
F(000)	340	376
Crystal size/mm^3	0.16 × 0.13 × 0.1	0.25 × 0.23 × 0.2
Radiation	MoKα (λ = 0.71073)	MoKα (λ = 0.71073)
2θ range for data collection/°	4.268 to 65.512	4.582 to 75.204
Index ranges	$-11 \le h \le 11$, $-13 \le k \le 13$, $-14 \le l \le 14$	$-12 \le h \le 12$, $-15 \le k \le 15$, $-15 \le l \le 16$
Reflections collected	9700	13 748
Independent reflections	4262 [R_{int} = 0.0357, R_{sigma} = 0.0485]	6458 [R_{int} = 0.0337, R_{sigma} = 0.0391]
Data/restraints/parameters	4262/0/165	6458/0/165
Goodness-of-fit on F^2	1.046	1.06
Final R indices [$I \geqq 2\sigma(I)$]	R_1 = 0.0342, wR_2 = 0.0684	R_1 = 0.0288, wR_2 = 0.0709
Final R indices [all data]	R_1 = 0.0461, wR_2 = 0.0726	R_1 = 0.0308, wR_2 = 0.0729
Largest diff. peak/hole/e Å^{-3}	0.58/−0.40	1.39/−1.28

cocrystal, there are strong C–H···N hydrogen bonding interactions between DPYA molecules that are not present in the DPYA-BrBF cocrystal, which will further strengthen the packing between DPYA molecules, resulting in a segregated stacking mode. However, the two cocrystals in this study adopt mixed packing modes and there are no strong interactions between DMCAT molecules. This is because the molecular structure of the fluorescent molecule DMCAT only contains one benzene ring, and it is difficult to have redundant positions to form strong interactions with the DMCAT molecule after forming a tight π–π stacking with the co-former molecule. Also, the types and ratios of interactions in both cocrystals are very similar, with the exception of slightly different halogen-bond interactions due to different halogen-bond donors, none of which are different. These reasons lead to the similar packing modes of the two cocrystals. Meanwhile, most of the halogen-bonded cocrystals reported so far are N···X halogen-bonded cocrystals, containing N···X interactions with distances of less than 3 Å in the majority of cases, in which nitrogen atoms are mainly derived from pyridine rings or other aromatic heterocycles, as shown in Table S1.† However, there are relatively few reports on O···X halogen-bonded cocrystals.[28,29] For the C═O···X halogen bond in the cocrystal prepared in this work, its interaction distance is greater than 3 Å, which may be resulted from the stronger electronegativity of the oxygen atom compared with that of the nitrogen atom.

To further analyze the non-covalent interactions present in the cocrystals, the FT-IR spectra were recorded to study the vibrational characteristics of the two cocrystals. As shown in Fig. S1,† the FT-IR spectra show that the cocrystals are complex compounds composed of corresponding monomers.[30] Compared with DMCAT form II, the carbonyl peaks in both cocrystals shift towards lower wavenumbers. This is due to the formation of halogen bond interactions in the cocrystals, resulting in elongated C═O bonds. Besides, DMCAT-2 has a larger redshift than DMCAT-1, indicating a stronger halogen bond interaction in DMCAT-2. These changes may be responsible for the differences in the photophysical properties of the cocrystals.

3.4. Theoretical simulation

CrystalExplorer was used to calculate the 3D Hirshfeld surfaces and 2D fingerprints, including the corresponding weak surface interaction contribution of the molecules. It was found from the Hirshfeld surfaces that the Br···O and I···O halogen bond interactions show a large area of dark red bright spots, suggesting relatively strong interactions in the cocrystals (Fig. S2(a and b)†). Other interactions, such as C···H, F···H, Br···H, and I···H interactions, show a small red bright spot, indicating that these interactions are weaker. It is worth noting that for the two cocrystals, their interaction types and proportions are very close, as shown in Fig. S2(c–f).† This may be attributed to similar structures of the two co-former molecules.

In order to fundamentally understand the driving force behind the formation of the cocrystals, especially the electronic properties of the atoms involved in weak interactions,[31] the molecular electrostatic potential of DMCAT and the two co-formers were calculated and visualized by Multiwfn and VMD software, as shown in Fig. S3.† The red and blue spheres represent positive and negative electrostatic potentials, respectively. The positive and negative potential values are represented by purple and green fonts, respectively, and the maximum and minimum values are highlighted in italics. As shown in Fig. S3,† the potential of the DMCAT molecule exhibits a crossed and symmetrical X-type charge distribution, with the maximum positive potential mainly concentrated on the hydrogen atom near the alkyl chain end (+20.41 and +20.65 kcal mol^{-1}, respectively), while the minimum negative potential mainly concentrated on the oxygen atom near the carbonyl group (−26.86 and −26.85 kcal mol^{-1}, respectively). The two co-formers exhibit similar and symmetrical charge distributions, both exhibiting a negative potential around the highly electronegative F atoms, and a positive potential around the Br and I atoms. According to the principle of complementary electrostatic potential, the extremely positive sites of the

electrostatic potential on the molecular surface tend to combine with the extremely negative sites, which can reduce the energy of the system to the greatest extent and cause it to be in the most stable state. In the area where hydrogen bonds and halogen bonds are formed, the van der Waals surface exhibits red and blue penetrating regions due to the electrostatic attraction. It is worth noting that for co-former 1, the maximum electrostatic potential is +23.33 kcal mol^{-1}, which is much lower than that of co-former 2 (+37.96 kcal mol^{-1}), and the minimum electrostatic potential of co-former 1 is −9.03 kcal mol^{-1}, which is greater than that of co-former 2 (−13.39 kcal mol^{-1}), indicating that co-former 2 may form stronger halogen bonds with DMCAT molecules. In addition, the positive potential (+22.93 kcal mol^{-1}) of the benzene ring center in co-former 1 is greater than that of co-former 2 (+18.09 kcal mol^{-1}), suggesting that there may be a tighter π–π stacking interaction in DMCAT-1.

4. Conclusions

In summary, two red-emissive cocrystals of DMCAT, DMCAT-1 and DMCAT-2, were prepared by selecting different halogen bond donors. Both cocrystals exhibit an isomorphic mixed packing mode, which is mainly due to their highly similar interactions and their proportions in the cocrystals. Besides, the two cocrystals exhibit enhanced quantum yields, which are mainly attributed to the dilution of DMCAT molecules by the insertion of the co-former molecules after the formation of mixed packing modes. This caused weakened π–π interactions between the DMCAT molecules in the cocrystals, which attenuates the aggregation-induced quenching effect. DFT theoretical calculations further confirmed that the excited state S_1 is mainly derived from the intramolecular charge transfer of DMCAT. Compared with DMCAT-1, DMCAT-2 has higher emission efficiency, which is due to the longer distance between the planes of the adjacent molecular benzene rings in DMCAT-2, despite similar proportions of C–C interactions of the two cocrystals. By combining SXRD, IR, Hirshfeld surfaces and molecular electrostatic potential analysis, it was found that the driving forces for the co-assembly of DMCAT and the co-formers are mainly halogen bonds, hydrogen bonds and π–π interactions. The photophysical behavior of pristine single-benzene fluorescent molecules was successfully optimized by a co-crystal strategy.

Conflicts of interest

There are no conflicts to declare.

Acknowledgements

This work was financially supported by the National Natural Science Foundation of China (grant number 21978201 and 22108196).

Note and references

1 Z. Huang and X. Ma, Tailoring Tunable Luminescence via Supramolecular Assembly Strategies, *Cell Rep. Phys. Sci.*, 2020, **1**(8), 100167, DOI: **10.1016/j.xcrp.2020.100167**.

2 X. Fang, X. Yang, D. Li, B. Lu and D. Yan, Modification of π–π Interaction and Charge Transfer in Ratiometric Cocrystals: Amplified Spontaneous Emission and Near-Infrared Luminescence, *Cryst. Growth Des.*, 2018, **18**(11), 6470–6476, DOI: **10.1021/acs.cgd.8b00470**.

3 D. Yan, A. Delori, G. O. Lloyd, T. Friscic, G. M. Day, W. Jones, J. Lu, M. Wei, D. G. Evans and X. Duan, A cocrystal strategy to tune the luminescent properties of stilbene-type organic solid-state materials, *Angew. Chem., Int. Ed.*, 2011, **50**(52), 12483–12486, DOI: **10.1002/anie.201106391**.

4 S. Du, S. Ma, B. Xu and W. Tian, Optical Waveguide and Photoluminescent Polarization in Organic Cocrystal Polymorphs, *J. Phys. Chem. Lett.*, 2021, **12**(38), 9233–9238, DOI: **10.1021/acs.jpclett.1c02726**.

5 B. Liu, Q. Di, W. Liu, C. Wang, Y. Wang and H. Zhang, Red-Emissive Organic Crystals of a Single-Benzene Molecule: Elastically Bendable and Flexible Optical Waveguide, *J. Phys. Chem. Lett.*, 2019, **10**(7), 1437–1442, DOI: **10.1021/acs.jpclett.9b00196**.

6 X. Li, S. Shen, C. Zhang, M. Liu, J. Lu and L. Zhu, Small-molecule based thermally activated delayed fluorescence materials with dual-emission characteristics, *Sci. China: Chem.*, 2021, **64**(4), 534–546, DOI: **10.1007/s11426-020-9908-5**.

7 Z. Zhang, E. Crovini, P. L. dos Santos, B. A. Naqvi, D. B. Cordes, A. M. Z. Slawin, P. Sahay, W. Brütting, I. D. W. Samuel, S. Bräse and E. Zysman-Colman, Efficient Sky-Blue Organic Light-Emitting Diodes Using a Highly Horizontally Oriented Thermally Activated Delayed Fluorescence Emitter. Advanced, *Opt. Mater.*, 2020, **8**(23), 2001354, DOI: **10.1002/adom.202001354**.

8 M. Shimizu and T. Hiyama, Organic fluorophores exhibiting highly efficient photoluminescence in the solid state, *Chem. – Asian J.*, 2010, **5**(7), 1516–1531, DOI: **10.1002/asia.200900727**.

9 Y. Chen, Y. Fang, H. Gu, J. Qiang, H. Li, J. Fan, J. Cao, F. Wang, S. Lu and X. Chen, Color-Tunable and ESIPT-Inspired Solid Fluorophores Based on Benzothiazole Derivatives: Aggregation-Induced Emission, Strong Solvatochromic Effect, and White Light Emission, *ACS Appl. Mater. Interfaces*, 2020, **12**(49), 55094–55106, DOI: **10.1021/acsami.0c16585**.

10 H. B. Yu, X. X. Song, N. Xie, J. X. Wang, C. L. Li and Y. Wang, Reversible Crystal-to-Crystal Phase Transitions with High-Contrast Luminescent Alterations for a Thermally Activated Delayed Fluorescence Emitter, *Adv. Funct. Mater.*, 2020, 2007511, DOI: **10.1002/adfm.202007511**.

11 S. Singha, D. Kim, B. Roy, S. Sambasivan, H. Moon, A. S. Rao, J. Y. Kim, T. Joo, J. W. Park, Y. M. Rhee, T. Wang, K. H. Kim, Y. H. Shin, J. Jung and K. H. Ahn, A structural remedy toward bright dipolar fluorophores in aqueous media, *Chem. Sci.*, 2015, **6**(7), 4335–4342, DOI: **10.1039/c5sc01076d**.

12 Y. Liu, A. Li, S. Xu, W. Xu, Y. Liu, W. Tian and B. Xu, Reversible Luminescent Switching in an Organic Cocrystal: Multi-Stimuli-Induced Crystal-to-Crystal Phase Transformation, *Angew. Chem., Int. Ed.*, 2020, **59**(35), 15098–15103, DOI: **10.1002/anie.202002220**.

13 L. Sun, Y. Wang, F. Yang, X. Zhang and W. Hu, Cocrystal Engineering: A Collaborative Strategy toward Functional Materials, *Adv. Mater.*, 2019, **31**(39), e1902328, DOI: **10.1002/adma.201902328**.

14 C. Zhai, X. Yin, S. Niu, M. Yao, S. Hu, J. Dong, Y. Shang, Z. Wang, Q. Li, B. Sundqvist and B. Liu, Molecular insertion regulates the donor-acceptor interactions in cocrystals for the design of piezochromic luminescent materials, *Nat. Commun.*, 2021, **12**(1), 4084, DOI: **10.1038/s41467-021-24381-5**.

15 Y. Sun, Y. Lei, H. Dong, Y. Zhen and W. Hu, Solvatomechanical Bending of Organic Charge Transfer Cocrystal, *J. Am. Chem. Soc.*, 2018, **140**(20), 6186–6189, DOI: **10.1021/jacs.8b00772**.

16 Z. Wang, F. Yu, W. Chen, J. Wang, J. Liu, C. Yao, J. Zhao, H. Dong, W. Hu and Q. Zhang, Rational Control of Charge Transfer Excitons Toward High-Contrast Reversible Mechanoresponsive Luminescent Switching, *Angew. Chem., Int. Ed.*, 2020, **59**(40), 17580–17586, DOI: **10.1002/anie.202005933**.

17 D. Wu, B. Zhang, Q. Yao, B. Hou, L. Zhou, C. Xie, J. Gong, H. Hao and W. Chen, Evaluation on Cocrystal Screening Methods and Synthesis of Multicomponent Crystals: A Case Study, *Cryst. Growth Des.*, 2021, **21**(8), 4531–4546, DOI: **10.1021/acs.cgd.1c00415**.

18 Y. Sun, Y. Lei, L. Liao and W. Hu, Competition between Arene-Perfluoroarene and Charge-Transfer Interactions in Organic Light-Harvesting Systems, *Angew. Chem., Int. Ed.*, 2017, **56**(35), 10352–10356, DOI: **10.1002/anie.201702084**.

19 A. Mandal, Y. Kim, S.-J. Kim and J. Park, Unravelling the fluorescence and semiconductor properties of a new coronene:TCNB charge transfer cocrystal polymorph, *CrystEngComm*, 2021, **23**(40), 7132–7140, DOI: **10.1039/d1ce00741f**.

20 L. Sun, W. Hua, Y. Liu, G. Tian, M. Chen, M. Chen, F. Yang, S. Wang, X. Zhang, Y. Luo and W. Hu, Thermally Activated Delayed Fluorescence in an Organic Cocrystal: Narrowing the Singlet-Triplet Energy Gap via Charge Transfer, *Angew. Chem., Int. Ed.*, 2019, **58**(33), 11311–11316, DOI: **10.1002/anie.201904427**.

21 W. Chen, S. Sun, G. Huang, S. Ni, L. Xu, L. Dang, D. L. Phillips and M. D. Li, Unprecedented Improvement of Near-Infrared Photothermal Conversion Efficiency to 87.2% by Ultrafast Non-radiative Decay of Excited States of Self-Assembly Cocrystal, *J. Phys. Chem. Lett.*, 2021, **12**(24), 5796–5801, DOI: **10.1021/acs.jpclett.1c01021**.

22 B. Tang, B. Liu, H. Liu and H. Zhang, Naturally and Elastically Bent Organic Polymorphs for Multifunctional Optical Applications, *Adv. Funct. Mater.*, 2020, **30**(40), 2004116, DOI: **10.1002/adfm.202004116**.

23 H. Liu, S. Zhang, L. Ding and Y. Fang, Dual-state efficient chromophore with pH-responsive and solvatofluorochromic properties based on an asymmetric single benzene framework, *Chem. Commun.*, 2021, **57**(33), 4011–4014, DOI: **10.1039/d1cc00718a**.

24 R. Huang, B. Liu, C. Wang, Y. Wang and H. Zhang, Constructing Full-Color Highly Emissive Organic Solids Based on an X-Shaped Tetrasubstituted Benzene Skeleton, *J. Phys. Chem. C*, 2018, **122**(19), 10510–10518, DOI: **10.1021/acs.jpcc.8b01251**.

25 Z. Xiang, Z. Y. Wang, T. B. Ren, W. Xu, Y. P. Liu, X. X. Zhang, P. Wu, L. Yuan and X. B. Zhang, A general strategy for development of a single benzene fluorophore with full-color-tunable, environmentally insensitive, and two-photon solid-state emission, *Chem. Commun.*, 2019, **55**(76), 11462–11465, DOI: **10.1039/c9cc06260b**.

26 X. Zhang, J. Wang, H. Liu, F. Yu, T. Wang, X. Huang and H. Hao, Polymorphism-dependent fluorescent emission, acid/base response and selective fluorescent sensor for Cu2+ ions based on single-benzene framework, *Dyes Pigm.*, 2022, **197**, 109903, DOI: **10.1016/j.dyepig.2021.109903**.

27 G. Bolla, Q. Liao, S. Amirjalayer, Z. Tu, S. Lv, J. Liu, S. Zhang, Y. Zhen, Y. Yi, X. Liu, H. Fu, H. Fuchs, H. Dong, Z. Wang and W. Hu, Cocrystallization Tailoring Multiple Radiative Decay Pathways for Amplified Spontaneous Emission, *Angew. Chem., Int. Ed.*, 2021, **60**(1), 281–289, DOI: **10.1002/anie.202007655**.

28 D. Cincic, T. Friscic and W. Jones, Isostructural materials achieved by using structurally equivalent donors and acceptors in halogen-bonded cocrystals, *Chemistry*, 2008, **14**(2), 747–753, DOI: **10.1002/chem.200701184**.

29 M. Zbačnik, M. Pajski, V. Stilinović, M. Vitković and D. Cinčić, The halogen bonding proclivity of the ortho-methoxy–hydroxy group in cocrystals of o-vanillin imines and diiodotetrafluoro-benzenes, *CrystEngComm*, 2017, **19**(37), 5576–5582, DOI: **10.1039/c7ce01332a**.

30 H. Sun, J. Peng, K. Zhao, R. Usman, A. Khan and M. Wang, Efficient Luminescent Microtubes of Charge-Transfer Organic Cocrystals Involving 1,2,4,5-Tetracyanobenzene, Carbazole Derivatives, and Pyrene Derivatives, *Cryst. Growth Des.*, 2017, **17**(12), 6684–6691, DOI: **10.1021/acs.cgd.7b01302**.

31 J. J. Du, S. A. Stanton, S. Fakih, B. A. Hawkins, P. A. Williams, P. W. Groundwater, J. Overgaard, J. A. Platts and D. E. Hibbs, Exploring the Solubility of the Carbamazepine–Saccharin Cocrystal: A Charge Density Study, *Cryst. Growth Des.*, 2018, **21**(8), 4259–4275, DOI: **10.1021/acs.cgd.8b01111**.